LASER INTERFEROMETER GRAVITATIONAL WAVE OBSERVATORY
- LIGO -
CALIFORNIA INSTITUTE OF TECHNOLOGY
MASSACHUSETTS INSTITUTE OF TECHNOLOGY

Technical Note	**LIGO-T11XXXXX–vX**	2012/08/29

Real-time Calibration of Gravitational-wave Strain

Eric R. Hendries

California Institute of Technology
LIGO Project, MS 18-34
Pasadena, CA 91125
Phone (626) 395-2129
Fax (626) 304-9834
E-mail: info@ligo.caltech.edu

Massachusetts Institute of Technology
LIGO Project, Room NW22-295
Cambridge, MA 02139
Phone (617) 253-4824
Fax (617) 253-7014
E-mail: info@ligo.mit.edu

LIGO Hanford Observatory
Route 10, Mile Marker 2
Richland, WA 99352
Phone (509) 372-8106
Fax (509) 372-8137
E-mail: info@ligo.caltech.edu

LIGO Livingston Observatory
19100 LIGO Lane
Livingston, LA 70754
Phone (225) 686-3100
Fax (225) 686-7189
E-mail: info@ligo.caltech.edu

http://www.ligo.caltech.edu/

1 Abstract

The Laser Interferometer Gravitational-wave Observatory (LIGO) uses a Fabry-Perot Michelson interferometer to measure the change in length between two test masses due to an incident gravitational-wave strain. Calibration of LIGO is necessary for a meaningful physical analysis of strains and their sources. Traditional calibration methods used multiple measurements of individual transfer functions of elements within the differential arm length control loop. A real-time calibration system has the advantage of taking the current state of the interferometers time-varying components, allowing for a more accurate calibration and smaller errors. Moreover, immediately having data in calibrated units will allow for quick identification of the type of gravitational-wave event, reconstruction of the source position, and notification of follow-up telescopes. We begin by simulating the control loop at the LIGO 40 meter prototype. This simulation then guides the real-time model that we implement in the digital control system to calibrate the interferometer while in operation.

2 Introduction

The Advanced Laser Interferometer Gravitational-wave Observatory (aLIGO) searches for gravitational-waves using a Fabry-Perot Michelson interferometer. These waves are predictions of General Relativity, but they have not been directly measured in the laboratory to date. Gravitational-waves are produced from the acceleration of a massive body, which may result from pulsations, collisions, or rapid orbital motion for example [1, 2]. Gravitational radiation propagates at the speed of light, and carries energy away from the radiating body. These waves should therefore be measurable with a ground-based detector such as aLIGO.

When a gravitational wave passes through aLIGO, it changes the length of each arm of the interferometer by different amounts. This change manifests itself in the dimensionless function of time $h(t)$, termed the gravitational-wave strain. The difference in arm lengths between the two Fabry-Perot cavities, ΔL, is the sum of contributions from the two polarization types 'plus', $+$, and 'cross', $\times$, of the gravitational wave

$$h(t) \equiv \frac{\Delta L(t)}{L} = F_+ h_+(t) + F_\times h_\times(t) \tag{1}$$

where F_+ and $F_\times$ are coefficients depending on the direction of the source and orientation of the detector, and L is the length of the instrument [1]. For a source mass M generating a gravitational wave, the strain is

$$h \sim \frac{GM}{Rc^2}\frac{v^2}{c^2} \tag{2}$$

where G is the gravitational constant, R is the distance from the observer, v is the speed of the object, and c is the speed of light [3]. Numerical values of the strain for reasonable sources, such as a black hole binary, are on the order of 10^{-22} to 10^{-23}. Measurement of this wave strain allows aLIGO to observe the waveform produced by various astronomical events. From these waveforms, many important physical parameters can be calculated. By making such measurements, scientists are able to use gravitational waves to study a plethora of astrophysical phenomena.

aLIGO will search for gravitational waves with frequencies between 10 and 10^4 Hz, opening a number of possible astrophysical sources for detection [3]. Chirp signals are produced by the spiral of a star into its binary partner such as a neutron star or black hole. The collapse of a Type II supernova can produce a burst signal if the collapse is not axially symmetric. Periodic signals may arise from the motion of neutron stars or pulsars. Even gravitational radiation from the very early universe may possibly be measured by correlating the stochastic signals of multiple detectors.

The strain sensitivity is the key factor determining the range of events that aLIGO can observe. The noise budget that limits the achievable strain sensitivity is shown in Figure 1, taken from [4]. With increased strain sensitivity, a greater variety of astronomical events are open to detection, and the rate of detections increases because the volume of space from which signals can be received is larger [1]. Increasing the light-storage time aids in sensitivity because the phase difference is greater when the interaction time between the gravitational wave and the light increases. Using a power recycling mirror to ensure that no light is lost back toward the laser source enhances sensitivity as well. The strain sensitivity is also improved by the large 4 km length of the interferometer because displacements from gravitational waves grow linearly with arm length while some types of noise do not [3].

Control of the various types of noise in the interferometer is highly important due to the small strains expected. Sensing noise is a result of limitations on sensing and recording the incident strain. Small motions of the suspended masses constitute the random force noise. Ultimately, measurements are limited by quantum noise. An important method used to reduce noise in the experiment is to apply feedback through control loops on measured quantities. This means that a variable is measured through the control signal necessary to hold it stationary [3].

Given the significance of this strain measurement, it is important that aLIGO be properly calibrated to observe astrophysical waveforms. This work will consider both simulations and digital implementation of a real-time calibration system on the 40 m LIGO prototype.

3 Calibration Principles

In the absence of sources producing any disturbance, the interferometer is held so that no light reaches the photodetector. The differential arm length change (the difference in length between the two Fabry-Perot cavities) is measured by monitoring the phase difference of light returning from each arm cavity. This phase difference is induced because the changing cavity length alters the cavity's resonant frequency relative to the laser frequency [1]. As a result of the length change, an error signal $e_D(f)$ is detected. This error signal as a function of frequency is related to the change in length by

$$\Delta L(f) = R_L(f) e_D(f) \tag{3}$$

where $R_L(f)$ is the length response function of the interferometer. Once this frequency-domain model has been established, the time-domain convolution kernel can be obtained and used to produce a measurement of $h(t)$ [5].

In order to characterize the length response function, the interferometers are conceptually

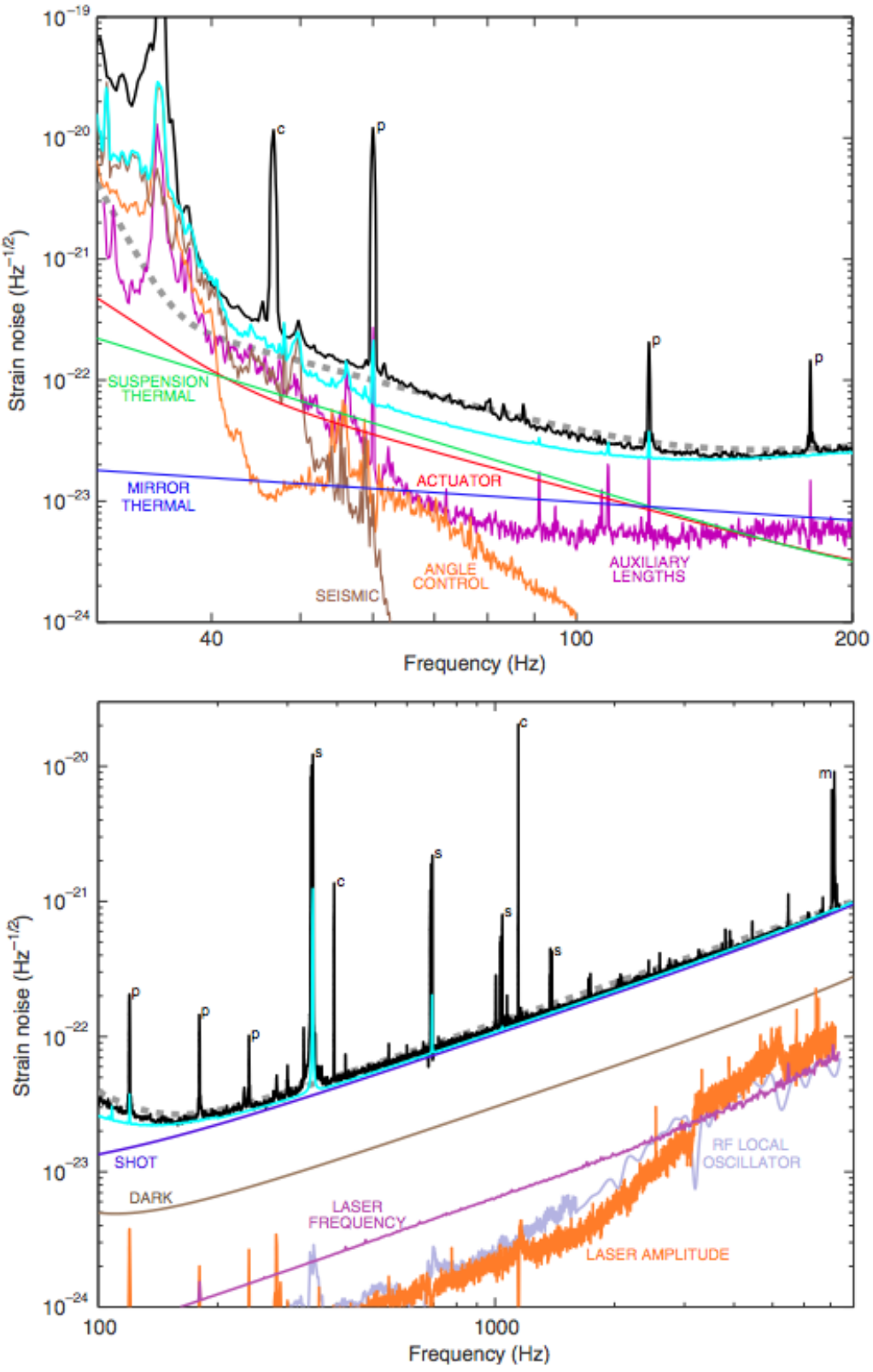

Figure 1: Strain sensitivity and noise budget for the S5 data run. Peak labeling is as follows: c denotes a calibration line, p is a power line harmonic, s indicates a suspension wire vibrational mode, and m is a mirror vibrational mode.

divided into subsystems of sensing, digital control, and actuation. Each of these subsystems is in turn composed of many components, all of which must be accurately calibrated. This is a tedious and time-consuming process in the traditional calibration methods. Further, it does not account for time-varying components of the control loop very well because all time-dependencies are lumped into one factor: the optical gain. As a result of these factors and others, it is advantageous to devise a different method of obtaining the length response.

Successful calibration of the interferometer requires knowledge of all three subsystems. Together they form a loop that controls the current state of the interferometer as it performs measurements. A detailed block diagram of the steps in this process taken from [6] is shown in Figure 2. First, the length sensing function $C_L(f)$ is a measure of how the interferometer responds to changes in arm lengths, and the digitization of that response. Next, a set of digital filters $D(f)$ is then used to produce a control signal from the loop error signal. Finally, the actuation function $A(f)$ then describes how the test masses respond to the digital control signal. The resulting model for the length response function is then

$$R_L(f,t) \equiv \frac{1+\gamma(t)C_L(f)D(f)A(f)}{\gamma(t)C_L(f)} \tag{4}$$

where $\gamma(t)$ records the time variation in the optical gain. The product

$$G = \gamma(t)C_L(f)D(f)A(f) \tag{5}$$

is called the open loop gain. The whole loop consists of a displacement of the end test mass causing a change in arm length that is then digitized, passing through digital filters, and conversion back into analog control through actuation of the end test mass [5].

Previous off-line calibration techniques used many measurements of each subsystem in order to obtain the length response function. The digital filter system is completely known. Frequency-dependent portions of the sensing and actuation functions can be directly measured, or are known from design schematics. An important measurement that sets the frequency-independent magnitude of the response function is that of the scale factor for the actuation function, K_A. These scale factors have previously been determined by using the free-swinging Michelson technique [5]. Devising a better way to make these measurements while in science mode is a major goal of this work.

4 Real-time Calibration

In order to extract the maximal information from astrophysical events, interferometer length and strain calibration will be performed in real-time through the digital control system. By using a real-time calibration method, the Advanced LIGO data acquisition system can be used to calibrate the gravitational wave data into strain while the experiment is in operation. We use the LIGO 40 m prototype interferometer at Caltech as a testbed for real-time calibration methods on one of the suspended arm cavities.

Calibration of the interferometer can be done in either the frequency or time domains. Initially, the calibration was performed in the frequency domain; later, algorithms were developed to calibrate LIGO in the time domain as well [7]. However, this method does not

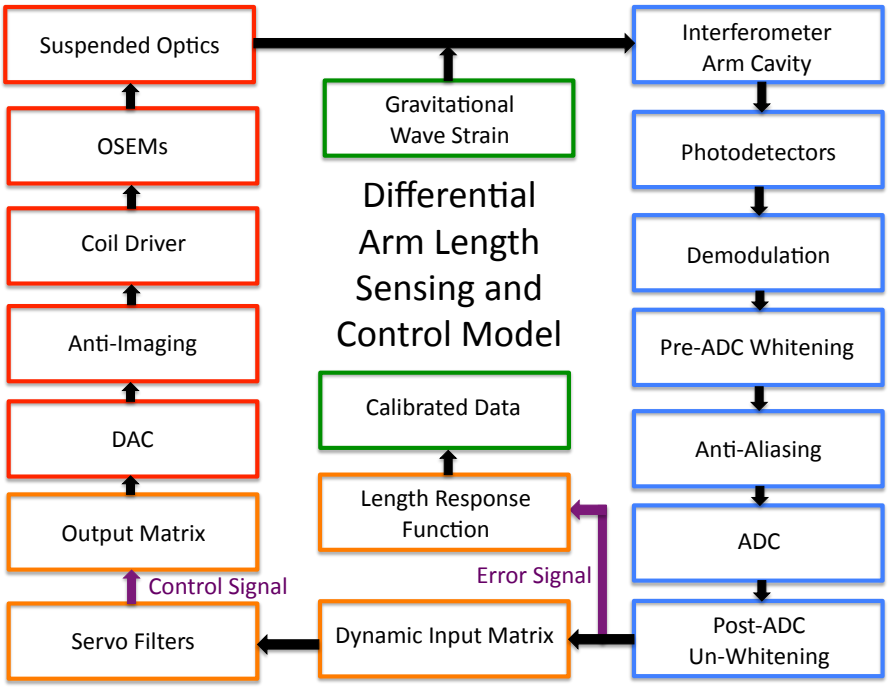

Figure 2: Block diagram of the components of the control loop for the differential end test mass displacement. The blocks within the length sensing function are blue, those within the digital function are orange, and those within the actuation function are red. ADC indicates an analog-to-digital conversion, DAC indicates a digital-to-analog conversion, and the OSEMs are optical sensor electromagnetic motors. The two most important signals for this work, DARM error and DARM control, are outlined in purple.

operate in real-time, but only after the time domain data is recorded in un-calibrated units. The goal of this work is not only to calibrate in the time domain, but to do this in real-time as well.

Some of the principles of calibration described above are incorporated into the real-time procedure also. However, under the old system, the measurements must be made prior to a science run and be registered as inputs to the model. For example, measurements made with the free-swinging Michelson technique cannot be done in real-time because the interferometer must be aligned in non-standard setups incompatible with normal operation.

The significance of real-time calibration is that it streamlines the process of measurement, linking observation and data analysis. The procedure also automatically incorporates any configuration changes, and allows for more control over systematic errors by producing a database of information on many interferometer components [8]. Moreover, immediately having data in calibrated units will allow for quick identification of the type of gravitational-wave event, reconstruction of the source position, and notification of follow-up telescopes.

5 Calibration System Simulations

As a way to establish a testbed for changes to the calibration systems, we employ computer modeling of the differential arm length sensing and control systems. In order to simulate the real-time calibration system, we use the Simulink modeling environment integrated with MATLAB. Salient features of the control loop incorporated in this model include the Fabry-Perot cavity itself, and the sensing, digital filtering, and actuation functions comprising the full feedback loop. From these systems the length response function may be obtained and used to recover the calibrated gravitational-wave strain [5]. A model of the interferometer control loop, including all of the components incorporated in the simulations presented here, is shown in Figure 2.

To construct a real-time calibration system, a database of information necessary to construct the calibration model must be established. Such data include the current status of digital filters and gains, previously measured transfer functions, and measurements of important open loop gains [8]. These data are treated as inputs to the real-time calibration model in Simulink, generating the length response function as output. The transfer functions of elements in the calibration model are taken from known design specifications as well as measurements taken in the laboratory. A time delay of 380 μs is also used in the model to obtain the correct phase-dependence of the loop.

The arm cavity is simulated using the results from [9], with parameter values relevant to the 40 m interferometer. This model uses the single pole approximation to obtain the frequency response of the arm cavity. Specifically, we calculate the transfer function for the signal at the anti-symmetric port in W/m, corresponding to the power received at the photodetectors given a differential arm displacement.

With all of the components of the control loop in place, the simulation may be checked for accuracy by using it to calculate the open loop gain. A comparison of the modeled and measured open loop transfer function is shown in Figure 3. The gain on this transfer function

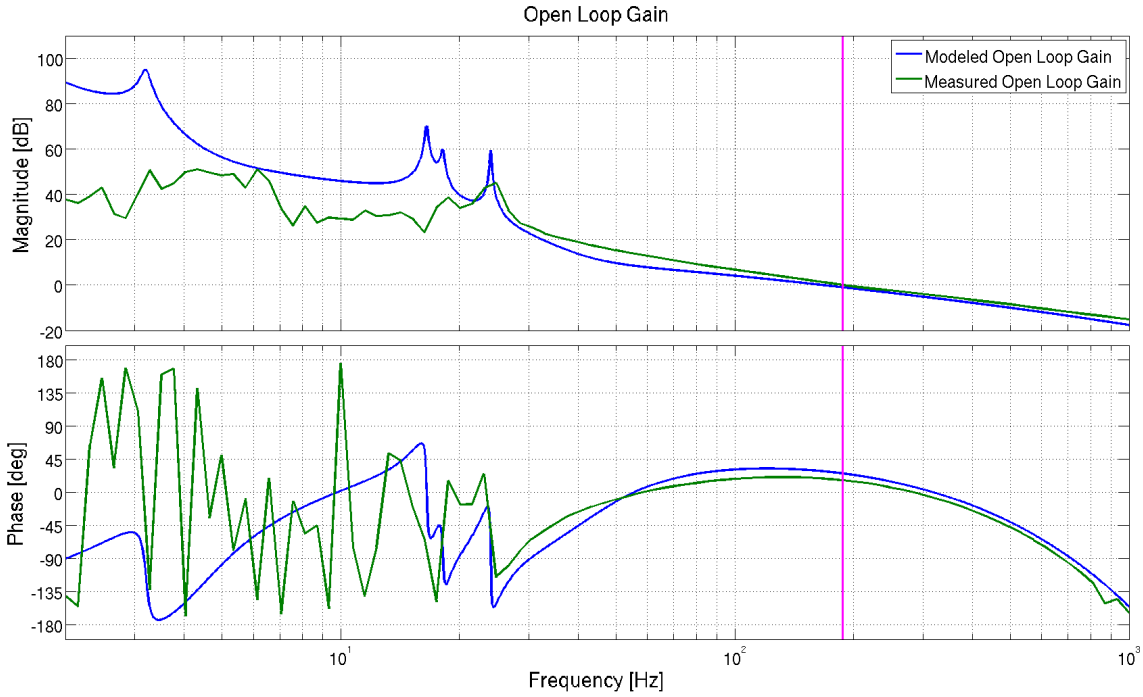

Figure 3: Comparison of the modeled and measured open loop transfer function. The model was scaled to fit the measured magnitude of the open loop gain at the unity gain frequency. The erratic behavior of the measured values low frequency is due to loss of coherence in measurement excitation signals.

was scaled to fit the measured value at the unity gain frequency. The measured values are erratic at low frequencies due to loss of coherence in the measurement excitations placed on the test mass. Obtaining this agreement between model and measurement is the benchmark test to validate the control loop simulations.

The vertical lines in Figure 3 indicate the location of the unity gain frequency, where the open loop transfer function has a gain of 1. The phase at this frequency is of critical importance. When the feedback loop is closed, there is a gain factor of

$$\frac{1}{1+G} \tag{6}$$

that is multiplied to blocks within the loop. If the phase is too close to -180° at the unity gain frequency, then $G \approx -1$, and this gain begins to diverge causing a loss of control of the interferometer. As a result, the servo filters in the digital control system are shaped so that the phase at the unity gain frequency lifts above -180°. The frequency range is bounded on the upper end by the Nyquist frequency, or half the sampling rate of the digital system. For the components in use at the 40 m, the sampling frequency is 16,384 Hz giving a Nyquist frequency of 8,192 Hz.

The individual functions that comprise the open loop transfer function are shown in Figure 4. The sensing function is dominated by the single cavity pole around 4.4 kHz for the 40 m interferometer. The digital function is the result of filter modules chosen so that the phase

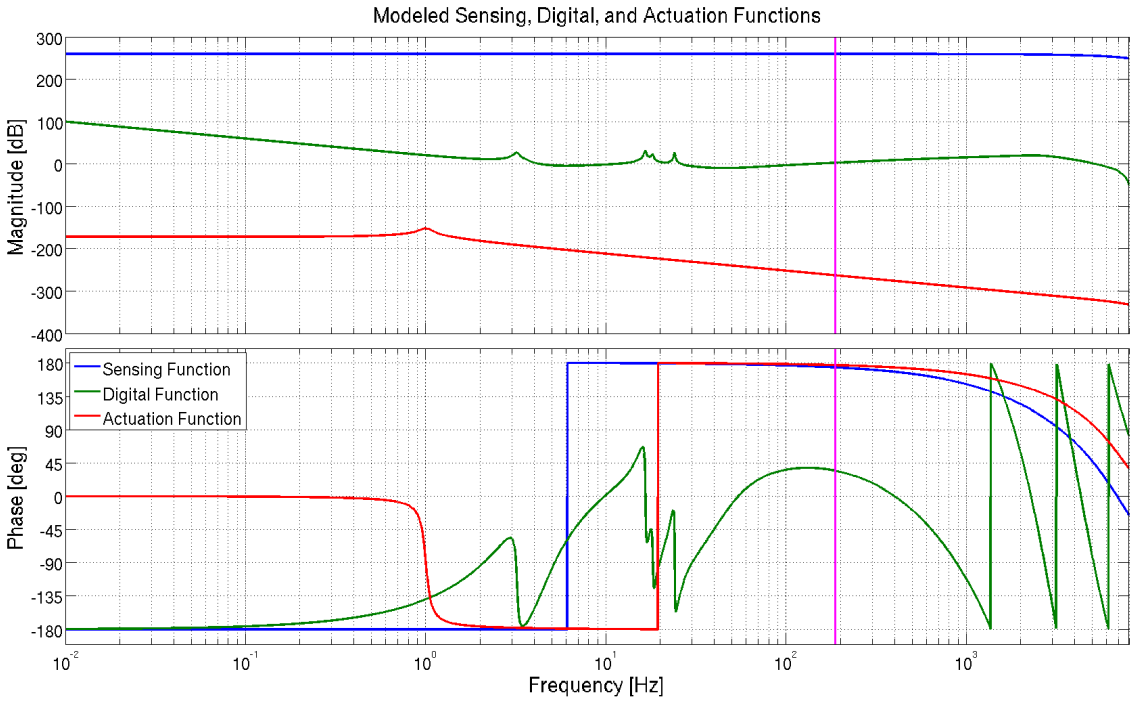

Figure 4: The components of the open loop transfer function in the arm cavity control loop. The vertical line is drawn at the unity gain frequency. The maximum frequency shown in the plot is the Nyquist frequency for the digital components in the loop. The large gains on the sensing and actuation functions are mostly due to the ADC and DAC systems having calibration factors of 10 V to 2^{16} counts or vice versa.

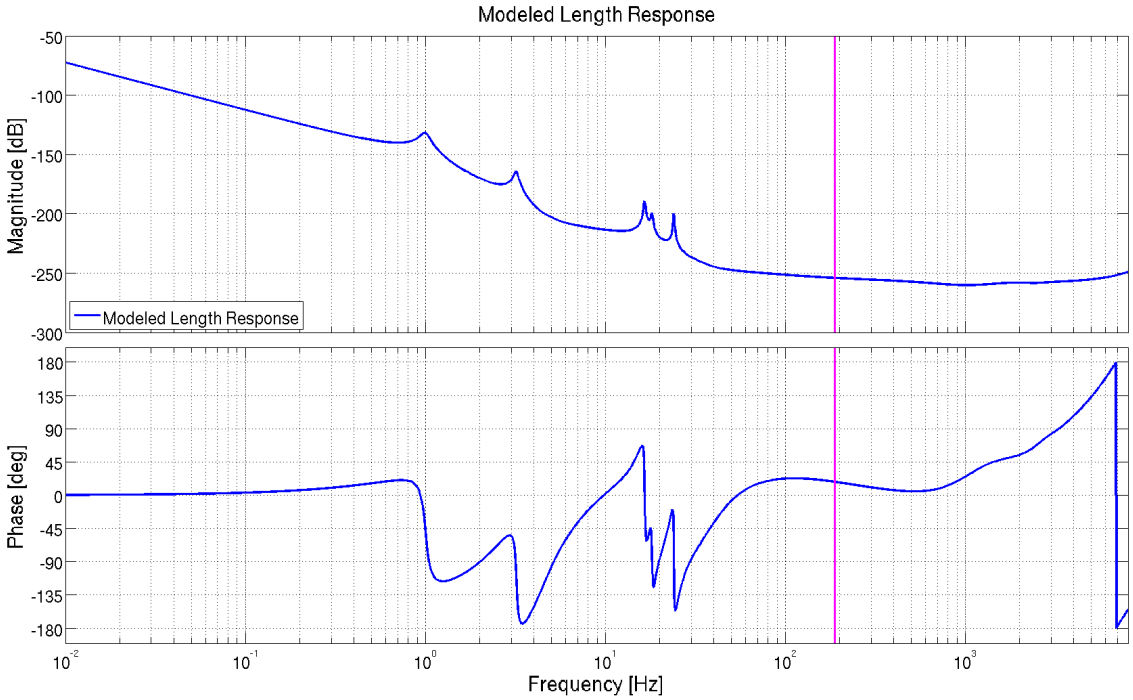

Figure 5: Simulated length response function from the Simulink model of the arm cavity control loop.

at the unity gain frequency meets the stability criteria discussd above. The characteristic feature of the actuation function is the pendulum transfer function of the suspended optics. From the open loop gain and sensing function output from the simulation, the length response function can be calculated as shown in Figure 5. With the simulated open loop transfer function validated by measurements, we can be confident that the length response function is accurate as well.

6 Digital Implementation

With the simulated off-line control loop validated with measurements, we use the calculated length response to calibrate the power spectrum of the arm cavity. The uncalibrated spectrum in units of digital counts is shown in Figure 6. After applying the length response, the calibrated spectrum is shown in Figure 7, now with the correct units of $\mathrm{m}/\sqrt{\mathrm{Hz}}$.

In addition to modeling the components of the length response function necessary for calibration, we have begun to implement the digital calibration system on one of the 40 m arm cavities. We will use the calibration system simulations discussed above to determine the form that the length response function should have in order to recover $h(t)$. This is accomplished by taking the error and control signals and passing them through a set of filters with the correct gain and frequency dependence so that the resulting sum forms the calibrated signal. The real-time model itself is also developed using Simulink. To include the model in the real-time digital control system, a custom C code conversion scheme is used

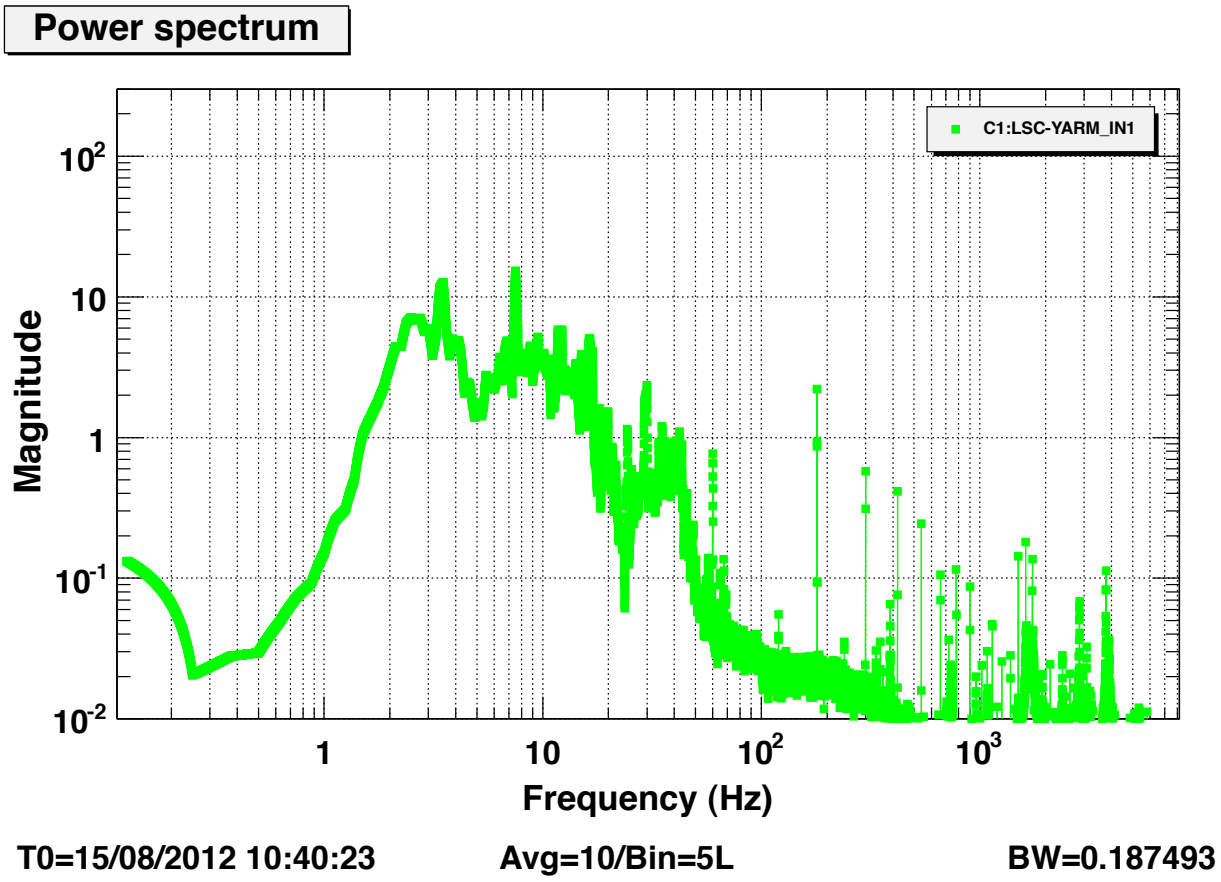

Figure 6: Uncalibrated power spectrum of the y-arm cavity at the 40 m lab. The units on the vertical axis are dimensionless counts from the digital control system.

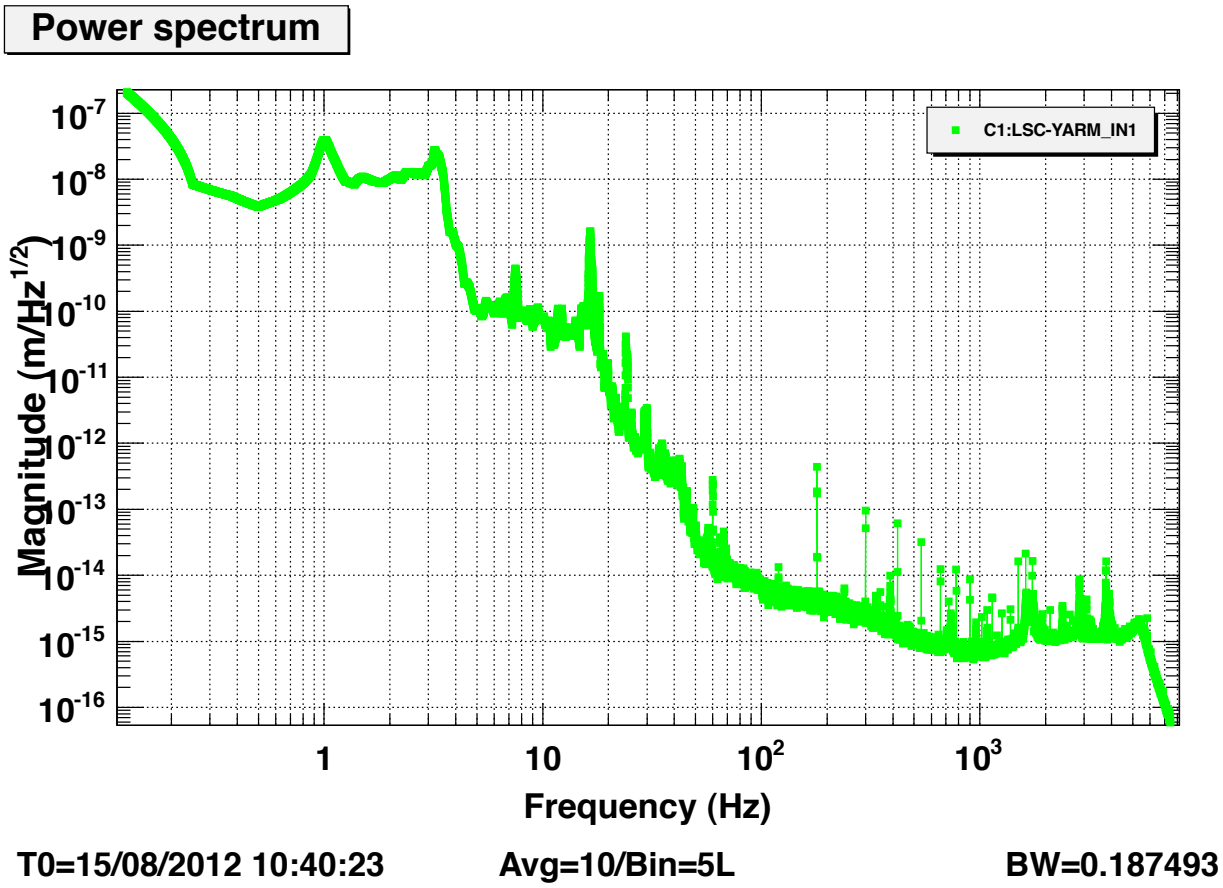

Figure 7: Calibrated power spectrum of the y-arm cavity at the 40 m lab.

that transforms the Simulink model into C. This code is then what ultimately manages the interferometer control systems.

We propose a real-time calibration system wherein the sensing function is considered time-dependent, but the digital and actuation functions are time-independent. The assumption of a time-independent actuation function is a simplifying, first-order approximation. The variability in the sensing function is accounted for by measuring the optical gain at certain calibration frequencies. By injecting calibration lines before and after the digital control system, we can form a measurement of the gain on the arm cavity transfer function as it varies in time. We take this measured optical gain and use its inverse value as a gain filter in the digital control system model for the length response. By doing this, the sensing function is scaled to the same value at all times, despite variations in the optical gain.

To see this mathematically, rearrange Equation (5) at the unity gain frequency where $G = 1$ to get

$$\frac{1}{D'} = \gamma' C_L' A' \tag{7}$$

where primes denote the value of a function at the calibration frequency. Now let u be the control signal and δ be the error signal (outlined in purple in Figure 2), so that $D' = u'/\delta'$. The inverse of the optical gain is then

$$\frac{1}{\gamma'} = C_L' A' \frac{u'}{\delta'}. \tag{8}$$

To measure this quantity physically, we propose to use a local oscillator applied to both the u and δ signals at the calibration frequencies, and include the result in the real-time calibration model.

7 Conclusions

We have presented a Simulink model outlining the requisite components and configuration of a real-time calibration system for aLIGO. Significant features of the model include all of the major components of the DARM length sensing and control loop. The transfer functions for these components were taken from known design values, measurements, and a model for the arm cavity. The calibration model is limited in that the magnitude of the open loop gain must be scaled to fit the measurements empirically.

We have also begun to implement a real-time calibration system at the LIGO 40 m prototype. With the results from the DARM control loop simulations, we are implementing a real-time model in the digital control system for one arm cavity. Directions for future work include further development of the real-time calibration model itself. Once this is fully established, the calibrations from the offline and online systems can be compared, and used to validate the real-time calibration.

8 Acknowledgements

I would like to thank Jamie Rollins and Rana Adhikari for their mentorship, and my fellow SURF students at the 40 m: Liz, Masha, Sasha, and Yaakov.

References

[1] A. Abramovici et al., *LIGO: The Laser Interferometer Gravitational-Wave Observatory.* Science 256, 325 (1992).

[2] J.D.E. Creighton and W.G. Anderson, *Gravitational-Wave Physics and Astronomy.* (2011).

[3] B.C. Barish and R. Weiss, *LIGO and the Detection of Gravitational Waves.* Phys. Today 52 (10), 44 (1999).

[4] B.P. Abbott et al., *LIGO: the Laser Interferometer Gravitational-Wave Observatory.* Rep. Prog. Phys. 72, 076901 (2009).

[5] J. Abadie et al., *Calibration of the LIGO gravitational wave detectors in the fifth science run.* Nuc. Ins. Meth. Phys. Res. A 624, 223 (2010).

[6] R. Adhikari, *Sensitivity and Noise Analysis of 4 km Laser Interferometric Gravitational Wave Antennae* (2004). LIGO-P040032-x0.

[7] X. Siemens et al. *Making $h(t)$ for LIGO.* Class. Quantum Grav. 21, S1723 (2004).

[8] V. Mandic et al., *S6 V2 Calibration Review* (2011). LIGO-T1100597-v1.

[9] D. Sigg et al., *Frequency Response of the LIGO Interferometer.* (1997). LIGO-T970084-00-D.

[10] P.R. Saulson, *Fundamentals of Interferometric Gravitational Wave Detectors.* (1994).